PARAMETRIC BASED AERODYNAMIC DESIGN OF PERFORMANCE ENHANCING BLADING SYSTEMS

Javid Bayandor
Sir Lawrence Wackett Centre for Aerospace Design Technology
Department of Aerospace Engineering, Royal Melbourne Institute of Technology
E-mail: javid.bayandor@rmit.edu.au

Keywords: *Advanced Propulsion, Fluid Power, HYPS, Propulsor,*

Abstract

In the present paper, a developed conceptual design for the blading systems of a large amplitude unsteady propulsion -HYPS- is described. The HYPS is an advanced Hydro-Propulsive System which confers upon its blading systems the ability to effectively receive the changing dynamics of the fluid environment. The paper continues by reviewing the analysis principles upon which the preliminary design was constructed. It further provides a general evaluation of the numerical method on the basis of system performance data gained through extensive trial.

1 Introduction

The status of the current turbomachinery technology indicates that the existing devices are incapable of controlling random and turbulent flow disturbing phenomena while maintaining the efficiency at the same time. This is partly due to the limitations of the conventional technology behind the design of such systems. The changes in the driving concept and the configurations used in turbomachinery systems for over a century have been too trivial to help advance such systems in correspondence with the extent of available and developing technology at the time.

The conventional systems use simple fixed or limited movable impellor blades, which are designed to deliver their best performance within fluxes flowing consistent to the direction of their blading systems. They can also handle some confined range of particular directional flow fields. In order to achieve high performances therefore, it is required for these turbine blades to be perfectly aligned with the direction of the flow. However, if the angle of impact changes, resulting in non-alignment of the blading systems to the flow, or the direction of flow diverts altogether, the turbines are no longer able to perform anywhere near their peak.

The advanced zero-head propulsion, *HYPS* [1], on the contrary to the conventional devices, confers upon its blading systems (propulsors) the ability to effectively receive the changing dynamics of the fluid environment.

Within this system, an optimised aerodynamic design of the complex configuration of the propulsors becomes of particular importance in enabling the blading to achieve enhanced power conversion efficiency within a wide range of flow regimes by constructively extracting the inflow energy.

This paper tends to provide an overview into some of the intricate analysis involved for finalisation of the propulsor design.

2 General Theory

2.1 Derivation of moment

In order to determine the initial forces and vortices generated by the system through its propulsors the following method was applied: it was assumed that an incompressible and inviscid fluid flows through the finite system - the *HYPS*- which was at rest at infinity with

respect to the selected Cartesian coordinate system (*x,y,z*). The mean velocity of this system, *S*, in the positive *x* direction was *U*, repeated after each time period τ or after each covered distance b:

$$b = U\tau\,. \tag{1}$$

The *HYPS* shares this time period with the surrounding flow field.

Assuming that vorticity was generated by *S*, it was proved that mean force could be exerted by *S* on the fluid [2]. In other words, the kinetic energy of the fluid was represented by the velocity field of the generated vorticity. When the periodically moving *HYPS* of finite extent induces a periodic neighbouring field of flow it can exert a mean force on the fluid which results in energy loss.

The mean value of the moment created around *x* axis due to the fluid pressure applied over the system *S* with respect to the origin *O* was derived using Eq. (2):

$$\begin{aligned}\frac{e_x}{\tau}\int_0^{\tau} M(t)\,dt = -\frac{\rho}{\tau}e_x \cdot \int_{\partial S}\big[\Phi(x+b,y,z,t+\tau)\\ \times\{(r(x,y,z,t)+be_x)*n(x+b,y,z,t+\tau)\}\\ -\Phi(x,y,z,t)\{r(x,y,z,t)*n(x,y,z,t)\}\big]\,dS\end{aligned} \tag{2}$$

where e_x is the unit vector in the *x* direction. As:

$$n(x+b,y,z,t+\tau) = n(x,y,z,t) \tag{3}$$

and the difference of the potential at corresponding points and times can be only a constant *c*, therefore:

$$\frac{e_x}{\tau}\int_0^{\tau} M(t)\,dt = -\frac{\rho c}{\tau}\int_{\partial S}\left(y\,n_z - z\,n_y\right)dS = 0 \tag{4}$$

In the simulation of the propulsor wings used in the *HYPS*, as it represented an actual system, a moment around a line through the mid points of the propulsor blade chords was also introduced.

2.2 Force generation

The mean value of the time dependent force *F* per unit of span exerted by the flow on the adaptive propulsor blade profiles over one period of time, τ, can be written as:

$$\begin{aligned}\frac{1}{\tau}\int_t^{t+\tau} F(t)\,dt &= \frac{1}{\tau}\int_t^{t+\tau}\left(F_x(t)+iF_y(t)\right)dt\\ &= \frac{i\rho}{\tau}\int_{\partial S}\{(\zeta+b)\,d\Phi(x+b,y,t+\tau)-\zeta\,d\Phi(x,y,t)\}\\ &= \frac{i\rho\,b}{\tau}\int_{\partial S} d\Phi(x,y,t) = \frac{i\rho\,b}{\tau}\,\Gamma\end{aligned} \tag{5}$$

where Γ is the circulation around the profiles, which represents a real number.

Therefore, from Eq. (5):

$$\begin{aligned}\frac{1}{\tau}\int_t^{t+\tau} F_x(t)\,dt = 0\,,\\ \frac{1}{\tau}\int_t^{t+\tau} F_y(t)\,dt = \frac{\rho b\Gamma}{\tau} = \rho U\,\Gamma\end{aligned} \tag{6}$$

2.3 Vorticity induction

For determining the vorticity induction, initially thin finite span propulsor blades were considered. The approach was constructed upon the following considerations and provided a different methodology to those of the conventional aero-hydrodynamically treated solutions.

It was initially assumed that the complex propulsor wings had very small thicknesses, their tips were rounded off and the main wing was parallel to a plane *y* = cte.

The rounding off of the blade tips created elliptic wing forms which are proven aero-hydrodynamically ideal shapes for the highly efficient wings with high lift to drag ratios. However, as the manufacturing process of such delicate wing shapes for the end product was not an economical practice, in the final optimum

design analysis, they were replaced by specific trapeziums. Such wings have a highly comparable performance to the elliptical ones due to their near "one" span efficiency factor, *e*. Moreover, their uncomplicated profiles introduced simplicity to the manufacturing process.

Further innovative and conventional efficiency enhancing measures enabled the control of the washout over the propulsor wing surfaces and the maintenance of the pressure difference between the upper and the lower sides of the wings hence, the lift force.

2.3.1 Vortex response of the equation of motion

To simplify the solution to the flow behaviour the following assumptions were made [3]: incompressibility and inviscid nature of the flow, flow divergence of $\theta = \theta(x, y, z, t)$, and flow vorticity of $\omega = \omega(x, y, z, t)$. It was also assumed that the flow passing the *HYPS* was limited to a finite region of unbound space. It was assumed that the velocity field was zero at infinity. Therefore, the unique solution to the behaviour of the flow around the *HYPS* will be:

$$v(x,y,z,t) = grad\,\Theta(x,y,z,t) + curl\,\psi(x,y,z,t) \tag{7}$$

where:

$$\Theta = -\frac{1}{4\pi}\int\frac{\theta}{R}\,dV\,,\quad \psi = \frac{1}{4\pi}\int\frac{\omega}{R}\,dV \tag{8}$$

and V denotes the volume.

To continue, it was supposed that $\theta = 0$ and ω was concentrated on a closed vortex line J along which a length parameter s was considered. Outside a narrow tube around J, $\omega = 0$ was assumed, where inside it $\omega \neq 0$. Its limit was considered homogeneously distributed while being tangent to J. Therefore, when σ is the area of the cross section of this tube:

$$\lim_{\sigma \to 0} \omega\sigma = \Gamma \tag{9}$$

From:

$$div\ curl\ v = div\,\omega = 0 \tag{10}$$

Γ, the vortex strength, is obtained. $\Gamma = |\Gamma|$ is constant along J. As the volume $dV = \sigma\,ds$ from Eq. (8):

$$\psi = \frac{1}{4\pi}\int\frac{\Gamma}{R}\,ds \tag{11}$$

Application of the operation *curl* to both sides of Eq. (11) with $(x, y, z) \notin J$, resulted in:

$$v = \frac{1}{4\pi}\int_J \frac{\Gamma * R}{R^3}\,ds = \frac{\Gamma}{4\pi}\int_J \frac{k * R}{R^3}\,ds \tag{12}$$

where $k = (d\xi/ds,\ d\eta/ds,\ d\zeta/d\,s)$ is the unit vector tangent to J. Equation (12) is the Biot-Savart law for a closed vortex line. Accordingly, the direction of Γ obeys the right hand rule against its locally induced velocities.

Outside the vortex line J, the fluid flow is free of rotation. The space outside J is simply connected to the inside space through a sufficiently smooth surface S bounded by the vortex line. A velocity potential considered was $\Phi = \Phi(x, y, z)$ where J and Γ were assumed to be independent of time; otherwise, Φ could have also been time dependent. Using the expression for k, and the x component v_x of v in Eq. (12), a relation for Φ was derived:

$$v_x = \frac{\Gamma}{4\pi}\int_J \left\{\frac{\partial}{\partial\zeta}\left(\frac{1}{R}\right)d\eta - \frac{\partial}{\partial\eta}\left(\frac{1}{R}\right)d\zeta\right\} \tag{13}$$

In the next step the Stokes' relation was applied:

$$\int_J g(\xi,\eta,\zeta)\cdot ds = \int_S (curl\ g)\cdot n\,dS \tag{14}$$

where $g = (g_x, g_y, g_z)$ is a vector field and n is the unit normal on S. The normal n obeys the direction of increase of s along vortex line J by the right hand rule. Applying the following in Eq. (14):

$$g_x = 0\,,\; g_y = \frac{\Gamma}{4\pi}\frac{\partial}{\partial\zeta}\left(\frac{1}{R}\right),\; g_z = -\frac{\Gamma}{4\pi}\frac{\partial}{\partial\eta}\left(\frac{1}{R}\right) \tag{15}$$

Eq. (13) was-written as:

$$v_x = +\frac{\Gamma}{4\pi}\frac{\partial}{\partial x}\iint_S\left(grad\,\frac{1}{R}\right)ndS = -\frac{\Gamma}{4\pi}\frac{\partial}{\partial x}\int_S\frac{R\cdot n}{R^3}dS \tag{16}$$

In this equation, the operator *grad* is taken with respect to *x, y, z*. As:

$$\Delta\frac{1}{R} = 0\,,\; (x,y,z)\neq(\xi,\eta,\zeta);\; \frac{\partial}{\partial x}\frac{1}{R} = -\frac{\partial}{\partial\xi}\frac{1}{R} \tag{17}$$

hence:

$$\frac{R\cdot n\,dS}{R^3} = \frac{\cos(n,R)\,dS}{R^2} \tag{18}$$

The right hand side of Eq. (16) represents the solid angle $d\Lambda$ under which the surface element d*S*, from the point (*x, y, z*) is seen. Hence, Λ is the total solid angle at (*x, y, z*) constructed by *J*:

$$v_x = -\frac{\Gamma}{4\pi}\frac{\partial}{\partial x}\Lambda \tag{19}$$

Applying the similar method, the other components (v_y and v_z) of *v* were determined.

For finding the potential function, the following was used:

$$\Phi = -\frac{\Gamma}{4\pi}\Lambda\,. \tag{20}$$

However, the function is not continuous over *S*.

This enabled a simple interpretation of vorticity generation in the *HYPS*: A small flat vortex ring of area *dS* and strength Γ at some point $Q(t_1)$, $t \geq t_1 \geq t_0$ was considered. The size of the ring was chosen with respect to the dimensions of the *HYPS*. At the centre of this ring, the unit normal *n* was assumed, related to Γ by the right hand rule. The differential potential $d\Phi$ of this vortex had the following value according to Eqs. (18) and (16):

$$d\Phi = -\frac{\Gamma}{4\pi}\frac{n\cdot R\,dS}{R^3} = -\frac{\Gamma}{4\pi}\frac{\cos\alpha}{R^2}\,dS \tag{21}$$

where α is the angle between *n* and *R*. It is seen from Eq. (21) that the small ring vortex is equivalent to a source doublet, in this case of strength ΓdS, with its axis in the *n* direction.

From Eq. (21) it follows that the potential function Φ can be determined as a superposition of potentials of small flat ring vortices of area *dS* and perpendicular to *f*(*s*) left behind the rotating *HYPS*. The vorticity Γ of such a ring is connected to the direction of *f*(*s*) by the right hand rule and has the following value:

$$\Gamma = \frac{1}{\rho}\frac{f(s)}{V(s)}\frac{ds}{dS} \tag{22}$$

It was required to consider the limits $ds \to 0$ and $dS \to 0$ for deriving the potential of these ring vortices. According to the theory of external force fields, the shape of the ring vortices is optional. For the purpose of simplicity in the solution, rectangular vorticity was considered.

In order to further elaborate on this vortex model, the singular force *f*(*t*) was split into two parts:

$$f(t) = h(t) + g(t) \tag{23}$$

Following, it will be shown that these forces somewhat represent the lift and drag forces caused by the fluid flow over the system on the propulsors. The components *h*(*t*) and *g*(*t*) were uniquely determined and, in linear stages of the analysis, the velocities induced by each of these forces were added to the fluid system to obtain the velocity field induced by *f*.

To calculate the strength of the vorticity shed behind the *HYPS*, the following was applied: the equations of motion for an inviscid

and incompressible fluid in an inertial Cartesian coordinates (x,y,z) were considered:

$$\frac{dv}{dt}=\frac{\partial v}{\partial t}+(v\cdot grad)\,v=-\frac{1}{\rho}gradp+\frac{1}{\rho}F \quad (24)$$

$$divv=0 \quad (25)$$

where an external force field per unit of volume is represented by $F = F(x,y,z,t)$ which acts on the fluid.

A flow field belonging to a force field around the *HYPS* was uniquely determined using appropriately chosen initial and boundary conditions. The force field at $t = 0$ was assumed to satisfy *curl* $F = 0$. This field was represented by:

$$F=grad\,\psi(x,y,z,t),\ t>0 \quad (26)$$

where ψ corresponds to some sufficiently smooth scalar function.

Equation (24) was therefore written in the form of:

$$\frac{\partial v}{\partial t}-v*\omega=-\frac{1}{\rho}grad\left(p+\tfrac{1}{2}|v|^2\right)+\frac{1}{\rho}F \quad (27)$$

where ω = *curl* v. By taking *curl* from both sides:

$$\frac{\partial\omega}{\partial t}-curl\,(v*\omega)=\frac{1}{\rho}curl\,F \quad (28)$$

As it is anticipated, this equation indicates that when *curl* $F \neq 0$ then $\omega \neq 0$. Therefore, given the fact that the rotation assumes a non-zero value, it was concluded that the resulting force field induced vorticity in the flow behind the *HYPS*.

Considering a closed contour $\tilde{C}$ in the fluid, it was assumed that the contour was coupled with the fluid particles passing through the *HYPS*. This resulted in its transport by the velocity field. At an instant of time, the circulation $\Gamma=\Gamma(t)$ of $\tilde{C}$ could be shown by:

$$\Gamma=\int_{\tilde{C}}v\cdot ds \quad (29)$$

where ds is a line element.

By partial integration:

$$\frac{d\Gamma}{dt}=\int_{\tilde{C}}\frac{dv}{dt}\cdot ds+\int_{\tilde{C}}v\cdot\frac{d}{dt}(ds) \quad (30)$$

where for the second integral:

$$\int_{\tilde{C}}v\cdot\frac{d}{ds}v\,ds=\frac{1}{2}\int_{\tilde{C}}\frac{d}{ds}|v|^2\,ds=0 \quad (31)$$

Using Eq. (24), the first integral also gave:

$$\frac{1}{\rho}\int_{\tilde{C}}(-gradp+F)\cdot ds=\frac{1}{\rho}\int_{\tilde{C}}F\cdot ds \quad (32)$$

Therefore:

$$\frac{d\Gamma}{dt}=\frac{1}{\rho}\int_{\tilde{C}}F\cdot ds \quad (33)$$

2.3.2. The perpendicular singular force h(t)

The significance of this singular force was that it could leave behind a vorticity perpendicular to its velocity and therefore was practically used to approximate the lift force of the propulsors.

By replacing the continuous action of the force with a singular forces $h(\sigma_n)$ acting during the time interval:

$$\int_{s_0}^{s_n}\frac{ds}{V(s)}\le t\le\int_{s_0}^{s_{n+1}}\frac{ds}{V(s)}. \quad (34)$$

During this time interval, the contribution of the singular force to the potential function will be of the magnitude of:

$$\Delta\Phi=-\frac{1}{4\pi\rho}\frac{h.R}{R^3}\frac{\Delta s}{V(\sigma_n)}. \quad (35)$$

This contribution is delivered by a little flat rectangular closed vortex, perpendicular to $h(\sigma_n)$, of length Δs and width $2\widetilde{\varepsilon}$. The strength of this vortex was derived using Eq. (22):

$$\Gamma = \frac{1}{\rho}\frac{h(\sigma_n)}{V(\sigma_n)}\frac{1}{2\widetilde{\varepsilon}} \tag{36}$$

where $h = |h|$.

By taking the limit $\Delta s \to 0$, and using Kutta-Joukowski theorem, the following vortex system was resulted:

$$\Gamma = \frac{1}{2\widetilde{\varepsilon}\rho}\left(\frac{d}{ds}\frac{h(s)}{V(s)}\right) \tag{37}$$

Using the Biot-Savart law, the velocity field induced by the vortex system was calculated, considering the velocity induction by both the starting vortex and the bound vortex and taking the limit $\widetilde{\varepsilon} \to 0$:

$$dv = \frac{1}{4\pi\rho}\int_{s_0}^{s_e}\frac{h(s)}{V(s)}\frac{d}{d\lambda}\left\{\left(i+\lambda\frac{dk}{ds}\right)*\frac{(R-\lambda k)}{|R-\lambda k|^3}\right\}\Big|_{\lambda=0} ds$$

$$= \frac{1}{4\pi\rho}\int_{s_0}^{s_e}\frac{h(s)}{V(s)}\left[3\frac{(R\cdot k)}{R^5}\cdot i * R + \frac{1}{R^3}\frac{dk}{ds} * R - \frac{1}{R^3} i * k\right] ds \tag{36}$$

Therefore, the velocity induction through the distributed vorticity using Eq. (22) was determined:

$$dv = \frac{1}{4\pi\rho}\int_{s0}^{se}\frac{d}{ds}\left(\frac{h(s)}{V(s)}\right)k * \frac{R}{R^3}\, ds\,. \tag{37}$$

2.3.3. The parallel singular force g(t)

In propulsion, force g, representing the drag force, often acts on the fluid in the negative s direction. Then, according to the Newton's third law, the force on the *HYPS* that causes g, is in the direction of the velocity V. In other words, this reaction introduces a propulsive force into the flow. Similar to the assumptions made in the previous case:

$$\Phi = \frac{1}{4\pi\rho}\int_{s_o}^{s_e}\frac{g(s)}{V(s)}\frac{d}{ds}\frac{1}{R}\, ds, \tag{38}$$

valid for all the coordinates which do not belong to the vortex ring. The magnitude of g is equal to $|g|$.

According to [4], this equation can be considered as a source system that produces a unit volume of fluid per unit time and has the velocity potential of:

$$\Phi = -\frac{1}{4\pi}\frac{1}{R}\,. \tag{39}$$

Hence, the propulsive force in the *HYPS* can be replaced by a sink.

By partial integration, from Eq. (38), the velocity field was determined:

$$v = \frac{1}{4\pi\rho}\left\{\frac{-gR}{VR^3}\Big|_{s_0}^{s_e} + \int_{s_0}^{s_e}\frac{R}{R^3}\frac{d}{ds}\left(\frac{g(s)}{V(s)}\right) ds\right\}$$
$$(x,y,z) \notin L \tag{40}$$

Further discussions concerning the satisfaction of the equation of mass conservation have been furnished by [5].

2.4. Influence of the propulsor downwash on the following propulsor

In the *HYPS*, the following propulsors operate within the trailing vortices springing from the leading propulsors ahead with the flow around them considerably influenced by these trails. The forces generated over the propulsor profiles, as seen from the trailing vortex drag equations, are proportional to the square of the velocity and the angle of incidence. Small velocity changes, therefore, have negligible effect unless they alter the incidence of the propulsor aerofoils. In this case, they then appear to have a significant effect on the generation of the force over the propulsors.

The following propulsors work at incidences that are altered appreciably by the tilting of the relative oncoming flow. This is due to the large downward induced velocity

components generated by the leading propulsors.

To calculate the effect of downwash on the following propulsors, it was assumed that the two consecutive propulsors were located a distance x apart. x, a distance vector, consisted of a vertical and a horizontal components, depending on the location of the origin and orientation of the coordinate system in used. For initial analyses, the second propulsor was assumed to be located behind the leading propulsor wing centre of pressure and in the plane of the vortex trail.

Assuming the near elliptic distribution, the semi-span of the bound vortex was [6]:

$$s' = (\pi/4)s \tag{41}$$

Downwash at the mid-span of the following propulsor, caused by the leading propulsor, was the sum of the downwash effects caused by the bound vortex and that of each of the trailing vortices. Using the Biot-Savart equations, the downwash at this point was determined as follows:

$$\begin{aligned} w_P \downarrow &= \frac{\Gamma_0}{4\pi x} 2\sin\beta + \frac{2\Gamma_0}{4\pi s'}(1+\cos\beta) \\ &= \frac{\Gamma_0}{2\pi}\left(\frac{\sin\beta}{x} + \frac{1+\cos\beta}{s'}\right) \end{aligned} \tag{42}$$

From the sketch $x = s'\cot\beta$ and $s' = (\pi/4)s$

$$w_P \downarrow = \frac{\Gamma_0}{2\pi}\left(\frac{\sin\beta}{s'\cot\beta} + \frac{1+\cos\beta}{s'}\right) = \frac{\Gamma_0}{2\pi s'}[1+\sec\beta]$$

$$w_P \downarrow = \frac{2\Gamma_0}{\pi^2 s}(1+\sec\beta) \tag{43}$$

Using the Kutta-Joukowski's theorem, and downwash angle:

$$\varepsilon = w_P / V \tag{44}$$

$$\varepsilon = \frac{2C_L VS}{\pi^3 s^2 V}(1+\sec\beta) \tag{45}$$

or,

$$\varepsilon = \frac{8C_L}{\pi^3 (AR)}(1+\sec\beta) \tag{46}$$

And:

$$\frac{\partial\varepsilon}{\partial\alpha} = \frac{\partial\varepsilon}{\partial C_L}\frac{\partial C_L}{\partial\alpha} = a_1\frac{\partial\varepsilon}{\partial C_L}, \tag{47}$$

hence:

$$\frac{\partial\varepsilon}{\partial\alpha} = \frac{8a_1}{\pi^3 (AR)}(1+\sec\beta) \tag{48}$$

This allowed the angle of attack of the following propulsor to be determined relative to the angle of attack of the leading one. The effect of the downwash on reduction of the latter angle of attack enables the following propulsors, operating within the wake region behind the leading propulsors, to reduce their drag generation, delay the flow separation over their low pressure wet surfaces, and control the stall phenomenon. [5] provides further details and analyses on the interacting effects and their significance on the overall performance of the system.

Having parametrically determined the forces, moments and velocity induction acting on the *HYPS* and its components, the motion could then be optimised. This was possible through introducing propulsor specifications that yield an optimum response within the equations.

3. Prototype Design and Manufacture

The results of the parametric study, while observing strict compliance with aero-hydrodynamic design guidelines, allowed the development of an optimum configuration for a *HYPS* prototype [5]. Subsequently, the scaled-down system was designed and constructed using rapid prototyping.

4. Comparison of Simulation and Test

The developed prototype of the *HYPS* was tested under different upstream flow conditions. This, together with detailed theoretical data analysis in the form of a parametric study, provided a better understanding of the complex fluid phenomena involved.

The test results were compared to the output of the numerical analysis of the simulated system, run under the corresponding initial conditions, to provide a basis for the evaluation of the numerical model. Different arrangements of the prototype represented the various modes of the simulation. These arrangements were constructed by alteration of the number of arms and rotors as well as a range of feedback controllers implemented within the system.

The comparisons made show a good level of agreement between the experiments and simulation. Figure 1. compares the power output between the numerical and experimental data in low Reynolds number conditions.

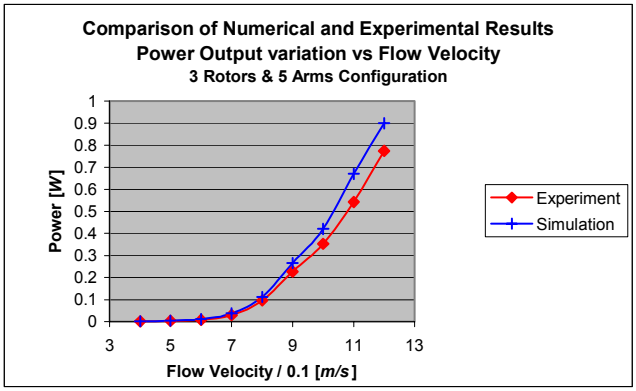

Figure 1. Comparison of experimental results with numerical analysis
(outside diameter of the *HYPS* prototype =0.26 *m*) [7]

Conclusion

The process of design and optimisation of the blading systems for an advanced unducted propulsion concept was described. The system offers a highly effective means for capturing the kinetic energy stored in a wide range of fluid motions, particularly random and turbulent.

The results of the investigation show that the system, as intended during the design process, maximises the prevailing aero-hydrodynamic forces on its impeller blades. It offers to eliminate the stall phenomenon on the propulsors altogether, or considerably delay it in very low upstream flow velocities. This enables the *HYPS* to enhance its rotary motion and achieve a higher energy conversion rate, which is in addition to its unique ability to capture energy from irregular and multi-directional flow particle movements.

In conclusion, the performance of an optimum configuration of the advanced propulsive system implies a significant increase in efficiency over the typical wind and hydro turbomachineries. The efficiency enhancement achieved is mainly owed to the parametric based aerodynamic design of the propulsors.

References

[1] Bayandor, J., Abanteriba, S., and Bates, I. 1999, 'A conceptual hydro-propulsive system for more efficient exploitation of fluid power', *Proceedings of the UNESCO's World Renewable Energy Congress 1999, WREC'99*, Kuala Lumpur.

[2] Hess, J. L., and Smith, A. M. O. 1967, 'Calculation of potential flow about arbitary bodies', *Progress in Aeronautical Science*, vol. 8.

[3] Potze, W., and Sparenberg, J. A. 1983, 'On optimum large amplitude sculling propulsion, finite span', *International Shipbuilding Progress*, vol. 30, no. 351.

[4] Batchelor, G. K. 1974, *An Introduction to Fluid Dynamics*, Cambridge University Press.

[5] Bayandor, J. 2000, A new zero head hydro-propulsive system, Ph.D. thesis, Royal Melbourne Institute of Technology, Melbourne.

[6] Anderson, J. D., Jr. 1991, *Fundamentals of Aerodynamics*, 2nd ed., McGraw-Hill, New York.

[7] Bayandor, J., Abanteriba, S., and Bates, I. 2001, 'An advanced zero head hydro-propulsive system', *Journal of Renewable Energy*, Elsevier Science, Oxford, vol. 24, pp. 475-484.